surfaces

MDPI

Article

4-Mercaptobenzoic Acid Adsorption on TiO_2 Anatase (101) and TiO_2 Rutile (110) Surfaces

Claudia Lorena Compeán-González [1,2], Andrew Guy Thomas [1,2,3,*], Karen Louise Syres [4], Jordan Cole [4] and Zheshen Li [5]

1 Department of Materials, School of Natural Sciences, The University of Manchester, Oxford Road, Manchester M13 9PL, UK; claudialorena.compeangonzalez@manchester.ac.uk
2 Photon Science Institute, Faculty of Science and Engineering, The University of Manchester, Oxford Road, Manchester M13 9PL, UK
3 Henry Royce Institute, The University of Manchester, Oxford Road, Manchester M13 9PL, UK
4 Jeremiah Horrocks Institute for Mathematics, Physics and Astronomy, School of Natural Sciences, Faculty of Science and Technology, University of Central Lancashire, Fylde Road, Preston PR1 2HE, UK; ksyres@uclan.ac.uk (K.L.S.); jcole4@uclan.ac.uk (J.C.)
5 Department of Physics and Astronomy, Centre for Storage Ring Facilities (ISA), Aarhus University, 8000 Aarhus, Denmark; zsli@phys.au.dk
* Correspondence: andrew.g.thomas@manchester.ac.uk

Abstract: The adsorption of 4-mercaptobenzoic acid (4-MBA) on anatase (101) and rutile (110) TiO_2 surfaces has been studied using synchrotron radiation photoelectron spectroscopy and near-edge X-ray absorption fine structure (NEXAFS) spectroscopy techniques. Photoelectron spectroscopy results suggest that the 4-MBA molecule bonds to both TiO_2 surfaces through the carboxyl group, following deprotonation in a bidentate geometry. Carbon K-edge NEXAFS spectra show that the phenyl ring of the 4-MBA molecule is oriented at 70° ± 5° from the surface on both the rutile (110) and anatase (101) surfaces, although there are subtle differences in the electronic structure of the molecule following adsorption between the two surfaces.

Keywords: titanium dioxide

Citation: Compeán-González, C.L.; Thomas, A.G.; Syres, K.L.; Cole, J.; Li, Z. 4-Mercaptobenzoic Acid Adsorption on TiO_2 Anatase (101) and TiO_2 Rutile (110) Surfaces. *Surfaces* **2022**, *5*, 238–250. https://doi.org/10.3390/surfaces5020017

Academic Editors: Gaetano Granozzi and Mohamed M. Chehimi

Received: 18 January 2022
Accepted: 28 March 2022
Published: 5 April 2022

1. Introduction

Over the last few decades metal oxides have attracted interest from both scientific and technological fields due to their properties such as wide band gaps, reactive electronic transitions, and dielectric constants, coupled with good optical, electrical, magnetic and electrochemical characteristics, amongst others [1–3]. Based upon these properties, a variety of technological devices is now possible. Additionally, key functional and structural properties of these materials can be tuned by several means, increasing the range of applications.

TiO_2 has become a model among metal oxides due its numerous applications, which range from everyday products such as a pigment in paints, plastics, cosmetics, and food, to advanced environmental and biomedical devices, thanks to its bandgap of 3–3.4 eV. TiO_2 lends itself to applications in fields such as photocatalysis, photovoltaics, fuel cells, batteries, biosensing, drug delivery and biomedical implants [2,4–6]. In many of the more advanced applications of TiO_2, the interaction of molecules is important and a number of studies of molecular interaction with TiO_2 surfaces, from simple molecules such as water to dye molecules such as those used in dye-sensitised solar photovoltaic (PV) cells, have been performed. [5,7,8]

Small organic molecules have been studied as linker molecules to facilitate charge transfer between polymers [9,10] or quantum dots (QDs) [11] and metal oxide surfaces [8]. In the solar PV applications, their ability to retard or prevent surface degradation of quantum dots is also of significant interest. PbS quantum dots have shown some promise

for solar harvesting and use in quantum dot sensitised solar cells (QDSSC). They have also been shown to exhibit multiple exciton generation, where two electrons are generated by the absorption of a single photon. However, they are susceptible to oxidation [12,13] and the ligands used to stabilise the dots tend to be rather insulating. The use of small aromatic molecules containing a carboxylic acid group, which is known to form a strong bond to titanium dioxide surfaces [8,14], may be a solution to this. In addition, the choice of a suitable functional group to bind to the QD is also important [15].

In this work we use X-ray photoelectron spectroscopy (XPS) and near-edge X-ray absorption fine structure (NEXAFS) spectroscopy to study the adsorption of 4-mercaptobenzoic acid (4-MBA) on the surfaces of two different TiO_2 polymorphs: rutile (110) and anatase (101). 4-MBA is a small aromatic molecule that contains two functional groups: a carboxylic acid and a thiol group (Figure 1), which together with other MBA isomers present potential advantages over their mercaptoalkanoic acid analogues for engineering surfaces of technological value [16]. It is anticipated that the carboxylic acid group will bind to the titania surface, leaving the thiol group free to interact with S-containing Q-dots, or with polymers such as poly 3-hexylthiophene, and in doing so improve the charge transfer between the light-harvesting moiety and the metal oxide, which may lead to an improvement in efficiency. Both titanium oxide polymorphs, anatase and rutile, are investigated due to their attractive applications. On one hand, rutile is the most common natural form of TiO_2; the (110) surface is the most stable surface of rutile and has been studied extensively. Rutile is also the phase which tends to form naturally on titanium, and therefore its interaction with organic/biomolecules is of significant interest. On the other hand, anatase TiO_2 (101) is the most stable anatase surface and is preferred for its optoelectronic applications and photocatalytic activity and is the usual form of TiO_2 in solar cell applications due to the relatively low synthesis temperatures used in the fabrication of solar cells. In addition, the nature of O-vacancies in these two polymorphs is subtly different. In rutile TiO_2 (110), the defects tend to occur in the so-called bridging oxygen rows [5]. O-vacancies in anatase TiO_2 (101), however, tend to form a subsurface [17]. Therefore, a comparison of the behaviour of molecular adsorption on these surfaces is of some interest.

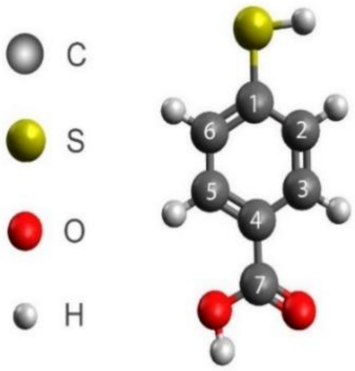

Figure 1. 4-mercaptobenzoic acid molecule representation. The grey spheres represent carbon atoms, the yellow sphere the sulphur atom and the red spheres the oxygen atoms. Numbering of carbon atoms is used for reference.

2. Materials and Methods

The experimental work was performed at the AU-MATLINE end station at the ASTRID2 Synchrotron facility at the Institute for Storage Ring Facilities (ISA) at Aarhus University. The beamline is equipped with a Scienta electron energy analyser and an SX-700 monochromator as well as instrumentation for Ar^+ ion sputtering and thermal annealing for sample cleaning and preparation. The base pressure in the end-station was around 5×10^{-10} mbar throughout the measurements.

TiO_2 anatase (101) and TiO_2 rutile (110) single crystals (PI-KEM Ltd.,Tamworth, UK) were mounted on two separate stainless-steel sample plates and held in place by two strips of tantalum wire. A thermocouple was attached to the sample plate, allowing monitoring

of the sample temperature during the experiments. The crystals were cleaned by repeated 1 keV Ar^+ ion bombardment and annealing to 700 °C in a vacuum until a sharp (1 × 1) LEED pattern was obtained, and the X-ray photoelectron spectra (XPS) showed the surfaces to be free from contaminants.

4-mercaptobenzoic Acid (4-MBA, Sigma Aldrich, Darmstadt, Germany purity 99%) powder was carefully degassed prior to use by gently heating in a glass dosing tube. To evaporate the 4-MBA into the vacuum chamber, the dosing tube and the line to the preparation chamber were heated from around 80 to 100 °C, while the single crystal was held at room temperature. Crystals were exposed to the vapour for between 20 min and 2.5 h. Coverage was calculated as described in the supporting information (Figure S1) and was found to be roughly constant on both surfaces at around 0.6 ± 0.1 nm, for all exposure times investigated here [18–20].

Photoelectron spectra were recorded at normal emission. For acquisition of the Ti 2p region, a photon energy of 560 eV was used, while O 1s spectra were recorded at 630 eV, C 1s at 385 eV and S 2p at 265 eV, all with a pass energy of 20 eV. This meant all core levels were recorded such that the emitted photoelectrons had a kinetic energy of ~100 eV, which means that a similar sampling depth is probed for all elements. NEXAFS spectra were recorded at incident photon angles of $25^\circ \leq \theta \leq 90^\circ$ relative to the surface. The NEXAFS spectra were recorded by detecting C K-edge Auger electrons at a kinetic energy of 270 eV in constant final state mode using the hemispherical analyser. During the recording of photoemission and NEXAFS spectra, the sample was held at room temperature.

All XPS data were analysed using Casa XPS software v2.3.24. Binding energies (BEs) were calibrated to the Fermi energy level from the Ta plate. A Shirley background was subtracted from the data, and Voigt curves (70:30% Gaussian/Lorentzian) were used to fit the core-level spectra [21]. All spectra are normalised to the most intense peak in the individual spectra. NEXAFS data analysis and peak fitting was performed using the IGOR Pro software v6.37 (WaveMetrics, Portland, OR, USA). Computer modelling was carried out using StoBe-deMon software v 3.3 [22] to perform density functional theory calculations of the excited C K-edge X-ray absorption spectra for the 4-mercaptobenzoic acid molecule.

3. Results and Discussion

3.1. X-ray Photoelectron Spectroscopy

Figure 2a shows the O 1s spectrum recorded from the clean TiO_2 anatase (101) surface. Two peaks appear at binding energies of 530.1 eV, which is assigned to the oxide and a second peak at 531.2 eV from oxygen atoms that are close to oxygen vacancy sites, or surface Ti–OH [23]. After 20 min of 4-MBA deposition, the oxide peak remains at a BE of 530.1 eV, but a second, more intense peak appears with a shift of 1.6 eV to higher BE, which is consistent with the COO− moiety of the 4-MBA molecule. This suggests adsorption on the anatase surface occurs through both oxygen atoms in the carboxyl group following the loss of the proton from the carboxylic acid group, as previously reported for other carboxylic acids [21,24]. After 2.5 h of deposition, a third peak appears at a BE of 533.4 eV. This peak is assigned to the chemically shifted C–OH group [25]. This behaviour would be consistent with the formation of a second layer, where the molecule is unable to adsorb dissociatively as the surface is already saturated with MBA. However, we note that for both the 20 min and 2.5 h exposures, the coverage remains constant at around 0.6 ± 0.1 nm. A simple geometry-optimised model of MBA, using a universal force field approach, shows the length of the free MBA molecule to be around 0.66 nm measured from the carboxylate group to the sulphur which, considering the tilt angle determined below, would be consistent with the 0.6 ± 0.1 nm coverage being a saturation monolayer. This may suggest that, at these long exposure times, a small portion of the molecules becomes adsorbed in a monodentate geometry in order to accommodate more molecules. This would also support the adsorption in a bridging bidentate mode as shown in Figure 3a, i.e., bound to two 5-co-ordinated Ti atoms rather than a chelating mode (Figure 3b), since only the former would result in more "free" Ti sites at the surface.

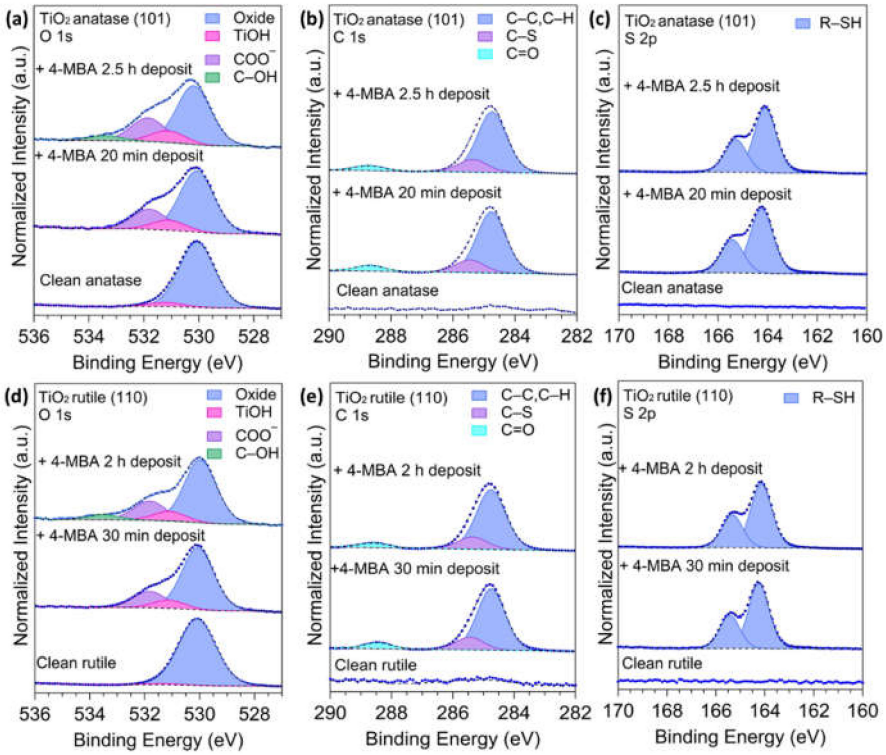

Figure 2. O 1s, C 1s and S 2p core-level synchrotron radiation photoemission spectra of (**a**–**c**) TiO_2 anatase (101) and (**d**–**f**) TiO_2 rutile (110) clean single crystals and following the deposition of 4-MBA. Spectra are normalised to the most intense peak. The doublets observed in the S 2p spectra are due to spin orbit splitting of the 2p state.

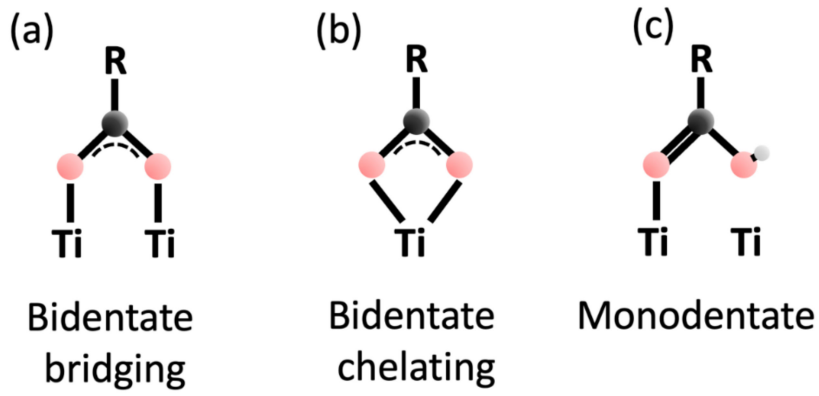

Figure 3. Schematic diagram showing (**a**) bidentate bridging, (**b**) bidentate chelating and (**c**) monodentate adsorption modes of an organic acid on a surface containing Ti. Red circles indicate carboxyl O atoms, black circles are C.

The C 1s spectrum recorded following the adsorption of 4-MBA on the TiO_2 anatase (101) surface is shown in Figure 2b and can be fitted with three peaks at BEs of 284.8 eV, 285.5 eV, and 288.7 eV. These peaks are assigned to carbon atoms C2−6 (284.8 eV), C1 (285.5 eV), and C7 (288.7 eV) as numbered in Figure 1. The S 2p spectra of 4-MBA adsorbed on anatase in Figure 2c show a spin–orbit split into a doublet with a branching ratio of 2:1 and an energy separation of ~1.2 eV. The two peaks at 164.3 eV and 165.5 eV, S $2p_{3/2}$ and S $2p_{1/2}$ respectively, arise from the R–SH group, further confirming that the molecule is adsorbed via the carboxyl group. The BEs and peak assignments for the adsorption of 4-MBA are shown in Table 1.

Table 1. Assignments of peaks fitted to the core spectra of clean TiO_2 anatase (101), 20 min of 4-MBA and 2.5 h 4-MBA deposit, their respective binding energies, and the relative abundances as a percentage of total areas. Percentage concentrations are quoted ±1%. * This peak arises from a combination of sites near surface O–vacancies/TiOH. For the dosed sample we have assumed that each molecule creates a single Ti–OH species. ** Positions for Ti 2p and S 2p doublets refer to the 3/2 peak.

Species	Assignment	Clean Anatase		20 min 4-MBA Deposit		2.5 h 4-MBA Deposit	
		BE (eV) ± 0.1	%	BE (eV) ± 0.1	%	BE (eV) ± 0.1	%
Ti 2p **	Ti^{3+}	456.9	8.1	457.2	7.6	457.1	7.8
	Ti^{4+}	458.6	91.9	458.7	92.4	458.9	92.2
O 1s	O Oxide	530.1	93.8	530.0	72.1	530.2	68.9
	TiOH *	531.2	6.2	531.1	9.31	531.1	8.6
	COO^-			531.8	18.6	531.8	17.5
	C–OH	-	-	-	-	533.4	5.0
C 1s	C2–6 (C–C, C–H)	-	-	284.8	77.1	284.7	77.7
	C1 (C–S)	-	-	285.5	15.9	285.4	16.0
	C7 (C–O)	-	-	288.7	7.0	288.7	6.3
S 2p **	R–SH	-	-	164.3	100	164.1	100

Photoemission spectra of the clean rutile TiO_2 (110) surface and following adsorption of 4-MBA are shown in Figure 2d–f. Similarities are found to the peaks obtained on the anatase surface. The O 1s spectrum recorded from the clean TiO_2 rutile (110) surface is again fitted with two peaks at BEs of 530.1 eV and 531.4 eV, corresponding to the oxide and sites associated with oxygen vacancies and surface Ti–OH. After 30 min of 4-MBA deposition, a peak associated with the deprotonation of the carboxyl acid group from the 4-MBA molecule is observed at a BE of 531.7 eV. Similarly, after 2 h of deposition of 4-MBA, a third peak at BE = 533.4 eV appears due to the presence of C–OH. Again, we suggest that this is due to a fraction of molecules adsorbed in a monodentate geometry at this higher exposure, for the same reasons as for the anatase surface.

The C 1s spectrum after adsorption of 4-MBA on the TiO_2 rutile (110) surface can be fitted with three peaks at binding energies of 284.8 eV (C–C), 285.4 eV (C–S), and 288.5 eV (C–O). The S 2p spectra recorded from the adsorbed 4-MBA, show spin–orbit split S $2p_{3/2}$ and S $2p_{1/2}$ peaks appearing at BEs of 164.3 eV and 165.5 eV, corresponding to the SH group. We note that a long deposition time does not lead to a shift in the position of the S 2p peak, which might be expected if a second layer or multilayers were formed. This would therefore be consistent with the discussion above, suggesting that in fact C–OH in the O 1s spectrum indicates a small fraction of monodentate-adsorbed MBA.

Table 2 summarises the peak positions, percentage contribution and assignment of the peaks recorded for the clean and 4-MBA dosed rutile TiO_2 (110) surface.

Table 2. Assignments of peaks fitted to the core spectra of clean TiO_2 rutile (110), 30 min of 4-MBA and 2 h 4-MBA deposit, their respective binding energies, and the relative abundances as a percentage of total areas. Percentage concentrations are quoted ±1%. * This peak arises from a combination of sites near surface O–vacancies/TiOH. For the dosed surfaces we have assumed that each molecule creates a single Ti–OH species. ** Positions for Ti 2p and S 2p doublets refer to the 3/2 peak.

Species	Assignment	Clean Rutile		30 min MBA Deposit		2 h MBA Deposit	
		BE (eV) ± 0.1	%	BE (eV) ± 0.1	%	BE (eV) ± 0.1	%
Ti 2p **	Ti^{3+}	457.5	4.6	457.3	5.0	457.0	4.9
	Ti^{4+}	458.7	95.4	458.5	95.0	458.6	95.1
O 1s	O Oxide	530.1	97.8	530.0	72.98	530.0	66.09
	TiOH *	531.4	2.2	531.1	7.58	531.1	8.01
	COO^-			531.8	19.44	531.8	20.54
	C–OH	-	-	-	-	533.5	5.37
C 1s	C2–6 (C–C, C–H)	-	-	284.8	76.6	284.8	77.9
	C1 (C–S)	-	-	285.4	15.9	285.4	16.1
	C7 (C–O)	-	-	288.5	7.5	288.6	6.1
S 2p **	R–SH	-	-	164.3	96.9	164.2	98.0

Figure 4 shows the Ti 2p core levels recorded from the anatase (101) and rutile (110) TiO_2 surfaces, both clean and following deposition of the 4-MBA molecule. For the clean anatase TiO_2 (101) surface, Figure 4a, the Ti 2p spectra consist of two peaks due to spin−orbit splitting: a Ti $2p_{3/2}$ peak at a BE of 458.6 eV and the Ti $2p_{1/2}$ peak at 464.3 eV. There is also evidence of residual Ti^{3+} from oxygen vacancies at 456.9 eV [23,26]. After the 4-MBA deposition, the Ti 2p spectrum shows a reduction in the intensity. Similar behaviour has been observed after the adsorption of other molecules on TiO_2 surfaces [21].

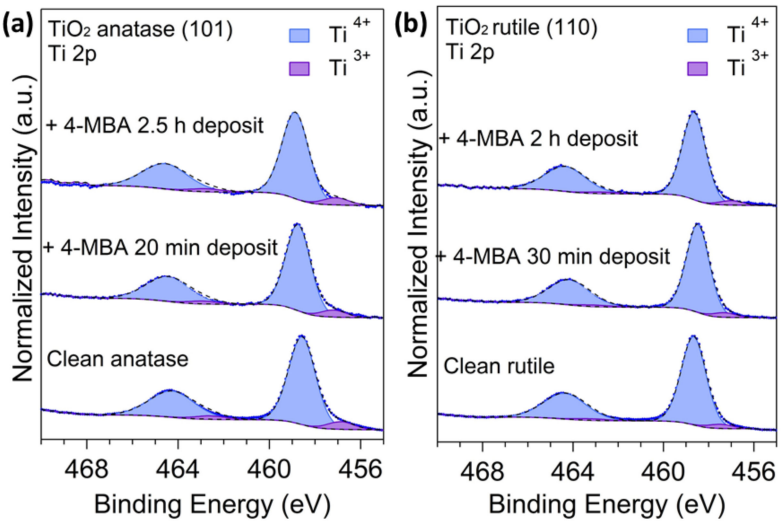

Figure 4. Ti 2p core-level synchrotron radiation photoemission spectra of (**a**) clean anatase TiO_2 (101) and (**b**) clean rutile (110) single crystals and following the deposition of 4-MBA.

Ti 2p spectra for the clean rutile (110) in Figure 4b show the Ti $2p_{3/2}$ peak at a BE of 458.7 eV and the Ti $2p_{1/2}$ peak at 464.4 eV. Residual Ti^{3+} from surface oxygen vacancies was also present, giving rise to a peak at 457.5 eV. For both anatase and rutile surfaces, it was found that adsorption of the 4-MBA molecule had no effect on the concentration of Ti^{3+} at the surface as shown in Tables 1 and 2, regardless of the deposition time.

The presence of defects, in the form of O–vacancies is important in adsorption on, and the catalytic activity of, titania. In anatase, it is widely believed that O–vacancies rapidly migrate below the surface but affect the electronic structure of the topmost surface [17,23]. These subsurface defects are thought to be behind the higher photocatalytic activity of anatase relative to rutile TiO_2 since adsorption on the surface does not lead to healing of the defect. For the rutile TiO_2 (110), on the other hand, surface O–vacancies are thought to occur predominantly on bridging O-rows and these tend to be filled by reaction with water forming two bridging –OH species (OHbr) [27]. Here, this water reaction may explain the lower initial concentration of O–vacancies in the rutile sample compared to the anatase crystal, due to reaction with residual water vapour in the vacuum system. One would expect a corresponding increase in the Ti-OH region of the O 1s spectrum, but this is obscured by the presence of the COO^- O 1s peak in this region. In both cases there is little change in the O-vacancy concentration upon adsorption. This is as expected, since organic acids are thought to predominantly bind to five-fold coordinated Ti at the surface [27]. The saturation coverage of MBA for both anatase (101) and rutile (110) seems to be constant at just over 1 monolayer (ML) even after >2 h exposure time, suggesting the defect density has little effect on the adsorption. It would be interesting to determine whether the initial adsorption rate is affected by defect density at the surface by using shorter exposure times and differing defect densities for the two phases.

3.2. UV Photoelectron Spectroscopy

Figure 5 shows partial and total density of states simulations for the 4-MBA molecule and Figure 6 shows a comparison with the valence band spectra for the clean anatase and rutile surfaces after the adsorption of the 4-MBA molecule.

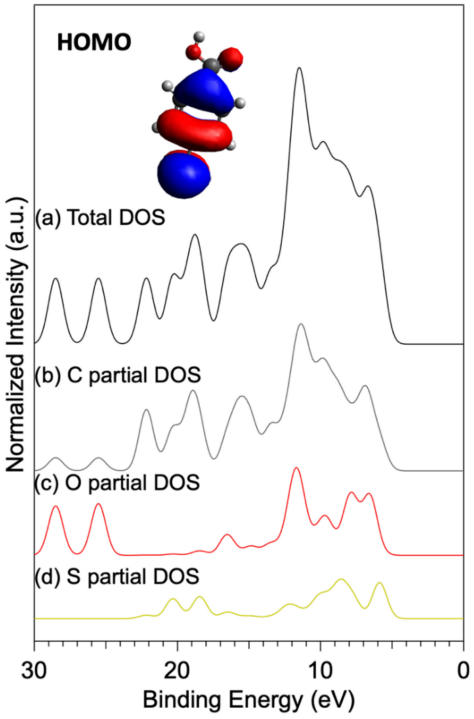

Figure 5. StoBe-calculated total density of states (DOS) and partial contributions of carbon (grey), oxygen (red), and sulphur (yellow) atoms in the 4-MBA free molecule. The HOMO molecular orbital of the 4-MBA molecule is displayed on the top left.

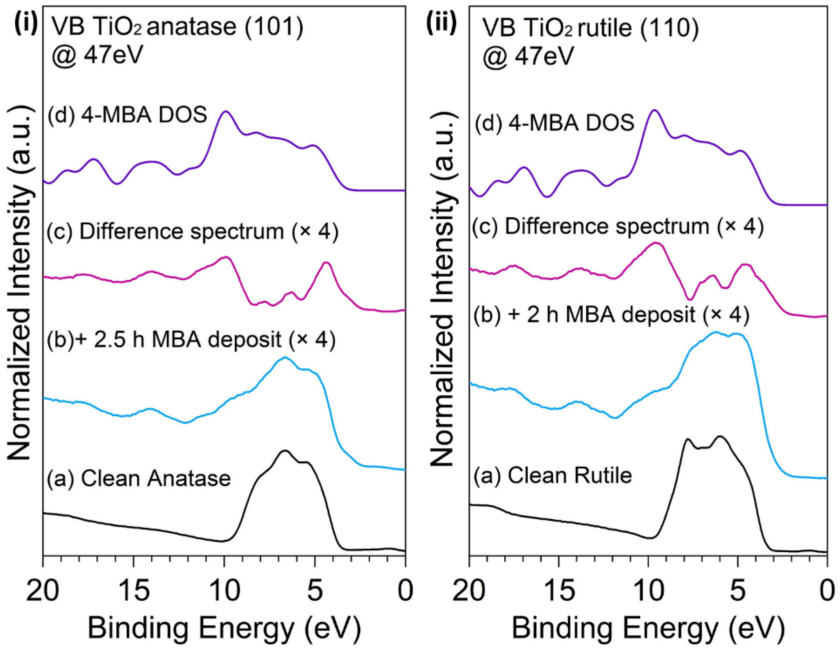

Figure 6. Valence band spectra recorded at 47eV from the (**i**) clean anatase, and (**ii**) clean rutile TiO_2 surfaces following the adsorption of the 4-MBA molecule.

The density of states (DOS) of the geometry-optimised 4-MBA molecule was calculated with the StoBe-deMon software (version 3.3) [28] using density functional theory (DFT). The molecular orbitals were calculated with the software ORCA (version 4.0) [29,30] and then visualised in Avogadro (version 1.2) [31]. The partial density of states simulations for carbon, oxygen, and sulphur (Figure 5b–d) show the contribution of the atoms in the 4-MBA total density simulation. As expected, carbon atoms have a major contribution to the total density of states simulation. The HOMO of the 4-MBA lies at approximately 6.67 eV with contributions from all atoms, but mainly carbon and oxygen.

Figure 6 displays a comparison of the 4-MBA DOS calculations (Figure 6i,ii(d)) with the difference spectrum (Figure 6i,ii(c) of the 4-MBA dosed surfaces (Figure 6i,ii(b)) and the clean TiO_2 surface spectra (Figure 6i,ii(a)).

The clean valence band spectra recorded at 47 eV (Figure 6i,ii(a)) is in good agreement with previous reports on the TiO_2 anatase (101) and rutile (110) surfaces with band gap states at around 1 eV, due to the presence of surface O-vacancies, and characteristic VB features at around 5 eV and 8 eV associated with the predominantly O 2p character of the valence band [32,33]. Changes on the spectrum following the adsorption of 4-MBA (Figure 6i,ii(b)) are more significant on the TiO_2 rutile (110) surface than in the anatase (101), where the band gap state remains after 2.5 h deposition time. Figure 6i,ii(c) show the difference spectrum, obtained by subtracting the clean spectrum from the 4-MBA dosed surfaces. Features from adsorption of the 4-MBA molecule appear at 4.34, 6.34, 7.85, 9.95, 11.45, 14.15 and 17.65 eV in the TiO_2 anatase (101) surface, and at 4.5, 6.4, 7.1, 9.6, 13.9 and 17.5 eV for the TiO_2 rutile (110) surface. Differences between both TiO_2 surfaces could be related to the availability of Ti and O atoms on the surface, including the oxygen vacancies of the anatase surface, and the amount of the 4-MBA molecule coverage. In addition, a shift to lower BEs of 1.65 eV and 1.9 eV can be observed for the anatase and rutile surfaces, respectively, when the StoBe-calculated spectrum was aligned to the experimental difference spectrum. In general, the experimental data show a fair agreement with the calculated DOS; however, the location of the molecular HOMO presents an additional shift to a lower energy of 0.68 eV for the anatase (101) and 0.27 eV for the rutile (110) surfaces, and there is a small difference in the intensity and width on the derived peaks. These differences can be related to the energy difference between the molecule in the gas phase (calculation) and upon adsorption on the TiO_2 surfaces. The larger shift in the predominantly molecular O 2p-derived HOMO for MBA adsorbed on anatase is linked to a stronger interaction of the molecule with the surface upon adsorption. Similar behaviour has been observed on previous studies of different molecules adsorbed on TiO_2 anatase (101) and rutile (110) surfaces [21,24,34].

3.3. Near-Edge X-ray Absorption Spectroscopy

Figure 7a shows a carbon K-edge angle-integrated NEXAFS spectra of 4-mercaptobenzoic acid adsorbed on TiO_2 anatase (101) and rutile (110), generated by summing spectra recorded at different incidence angles, compared to the StoBe generated NEXAFS spectrum. For the calculation, X-ray absorption spectra at the C K-edge are calculated for each atom individually (Figure 7b), and then summed to give the total spectrum. The labels, C1–C7, correspond to the numbered atoms in the ball-and-stick model. The experimental NEXAFS spectra are in good agreement with the calculated StoBe NEXAFS spectrum for the 4-MBA molecule.

The experimental spectra exhibit three clear shape resonances, at 284.8 eV, 285.2 eV and 288 eV which correspond to the C $1s_{C–C} \rightarrow \pi^*_a$ (284.8 eV), C $1s_{C–S} \rightarrow \pi^*_a$ and C $1s_{C–C} \rightarrow \pi^*_b$ (285.2 eV), and C $1s \rightarrow \pi^*_a$ and C $1s_{C–S} \rightarrow \pi^*_b$ (288 eV) transitions [16,19], respectively, as shown in the energy level diagram in Figure 7c. Lee et.al. [16] attributed the difference of energy between the π^* resonances from the aryl and carboxyl atoms to the effect of the oxygen atoms from the carboxyl group of the mercaptobenzoic acid (MBA) molecule, leading to an increase in binding energy of the C 1s initial state. Furthermore, a single peak from the carboxylate group is consistent with the molecule bonding in a bidentate mode to surface titanium atoms in agreement with the photoelectron spectra results [19]. Figure 7d

shows the lowest unoccupied molecular orbital (LUMO) and LUMO + 1 calculated by ORCA (version 4.0) [29,30] and visualised in Avogadro (version 1.2) [31].

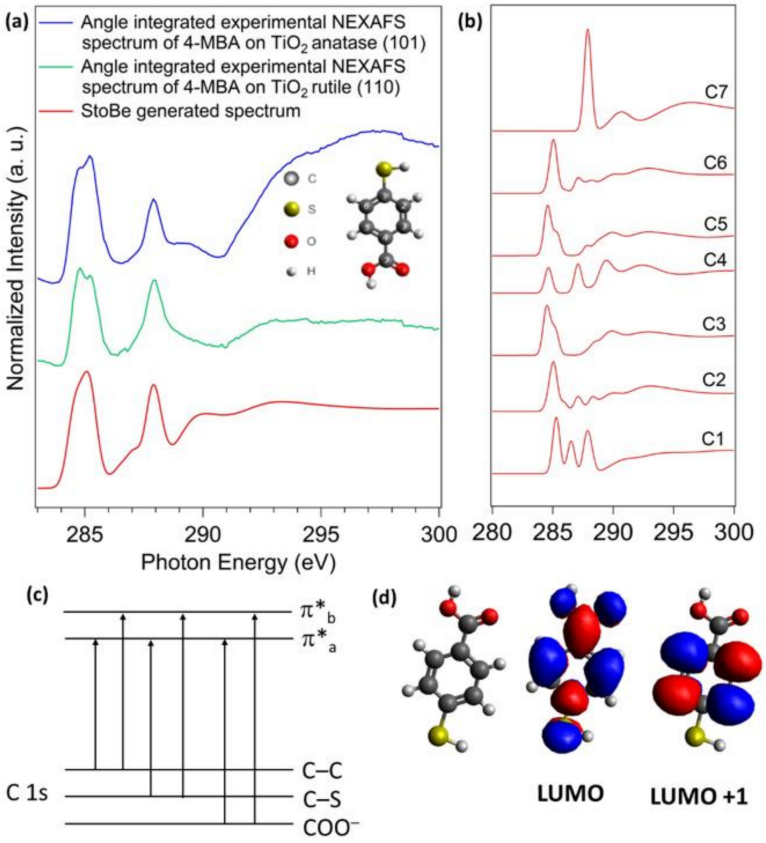

Figure 7. (**a**) Carbon K-edge NEXAFS spectra of 4-mercaptobenzoic acid adsorbed on anatase TiO_2 (101) and rutile (110) surface and a StoBe-generated NEXAFS spectrum. The panel on the right (**b**) shows the individual contributions of each carbon atom to the NEXAFS spectrum. Labels C1–C7 refer to the numbers in the molecular diagram shown as the inset in (**a**). (**c**) Energy level diagram showing the key electronic transitions for the NEXAFS process in the C 1s → π* region. (**d**) Molecular orbitals.

When the experimental data are compared with the calculation, we can observe that the first two peaks, π_a and π_b, are not as well-resolved in the calculated 4-MBA molecule spectrum. This may arise due to a slight shift in the positions of the two π^* features contributing to the spectrum here, which can arise due to slight changes in the initial or final state energies of the energy levels involved [35]. This is likely to be due the interaction of the 4-MBA with the TiO_2 surfaces, which is not considered in the calculation. We also observe differences in intensity of the peaks π_a and π_b when adsorbed on the anatase (101) and rutile (110) surfaces. We believe this to be linked to the strength of interaction of the molecule with the different surfaces. The valence band difference spectra in Figure 6 also show some minor differences in the valence band structure of the molecule for the two surfaces in the region around 6–7 eV binding energy, which the pDOS calculations show are predominantly linked to O-states in the molecule. It can be seen for the anatase (101) surface these molecular O 2p states have a larger splitting than for the calculated O-pDOS. Adsorption on the rutile surface, however, appears to have little effect on the splitting of these states. This indicates that there are subtle changes in the interaction of the molecule with the two TiO_2 surfaces studied, which leads to a larger effect on the molecular O 2p states in the case of the anatase surface, perhaps suggesting a stronger interaction.

Figure 8 shows angle-resolved carbon K-edge NEXAFS spectra of the 4-MBA molecule on TiO_2 anatase (101), Figure 8a, and rutile (110), Figure 8b, recorded for angles of incident radiation at 25–85° to the surface. The spectra are normalised by dividing the 4-MBA-

dosed TiO_2 C K-edge NEXAFS spectra by a clean gold C K-edge NEXAFS spectrum to remove photon flux features. Then, the step edge at the ionization potential on the resulted spectra is set equal to unity. The angle-resolved NEXAFS spectra allow us to determine the orientation of the 4-MBA molecule following adsorption onto the titania surfaces, by fitting Stöhr equations [35] to the data points. The solid line in Figure 8c displays the best fit for the anatase (101) data, giving an angle of the π^* orbital of $20 \pm 5^\circ$ from the surface, with the plane of phenyl ring oriented at $70 \pm 5^\circ$ to the surface. Similar calculations for the rutile (110) give a tilt angle of the ring of $66 \pm 5^\circ$ from the surface. Unfortunately, the error is likely to be quite large since only one azimuthal angle could be measured [35].

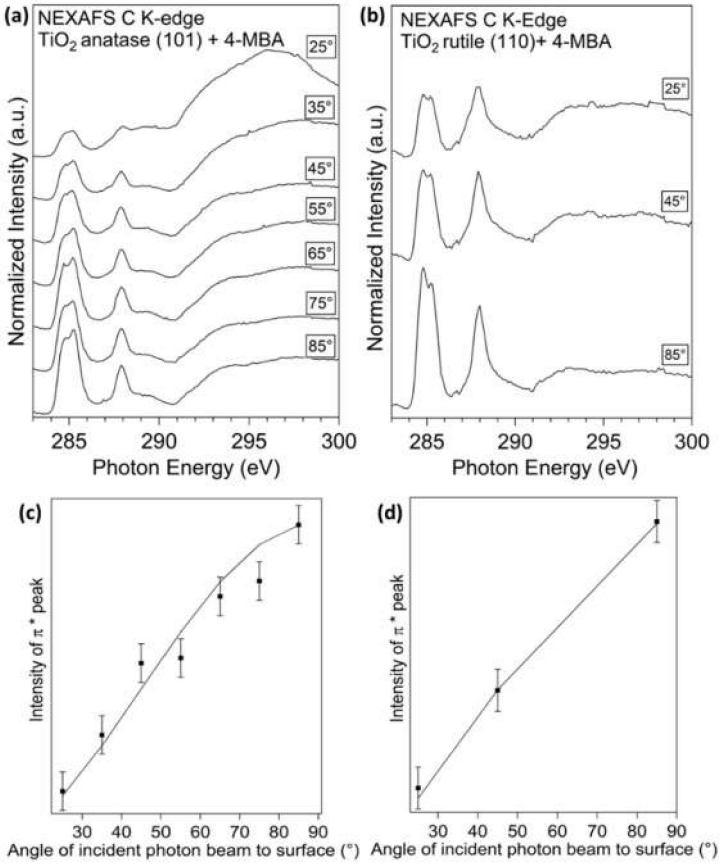

Figure 8. Carbon K-edge NEXAFS spectra recorded from (**a**) 20 min of 4-MBA deposit on anatase (101) and (**b**) 30 min 4-MBA deposit on rutile (110) surface. Intensity of the π_a * peaks (normalised to 1) vs the angle of the incident photon beam with respect to the surface. The solid line is a best fit to the data using Stöhr equations [35] from (**c**) anatase (101) and (**d**) rutile (110) surfaces.

The results above suggest the adsorption geometry of 4-mercaptobenzoic acid is similar on the rutile and anatase surfaces, although there appears to be a difference in the strength of interaction. The orientation of the molecule, with bonding through the carboxyl group in a bidentate geometry, leaves the thiol free, which may be useful in attaching other molecules, or indeed nanoparticles, such as Au, to the surface for catalytic applications. The valence band and NEXAFS spectra suggest there are small differences in the electronic structure of the molecule adsorbed on the two surfaces, which is likely to be linked to the degree of interaction with the surface. Further work is required to study this in more detail. In particular, it would be useful to study the charge transfer rate between the molecule and the two surfaces, as this may give an indication of the degree of hybridisation between the molecule and oxide surface. It would also indicate whether this stronger hybridisation between the molecular state and the oxide enhances charge transport at the interface, which would be beneficial for dye-sensitised or hybrid solar cells. This is because rapid charge

transport at the interface reduces the possibility of recombination of the photoexcited electron and hole.

4. Conclusions

Photoemission results show that the 4-mercaptobenzoic acid (4-MBA) molecule adsorbs on TiO_2 anatase (101) and rutile (110) surfaces in a bidentate mode, following the deprotonation of the carboxyl group, and that the geometry in terms of the tilt angle of the molecule is similar for the two surfaces. The data also suggest that the molecule is more strongly bonded to the anatase surface, since the molecular O-derived valence states are seen to shift to higher energy. Carbon K-edge NEXAFS spectra indicate the plane of the phenyl ring of the molecule to be tilted $70 \pm 5^{\circ}$ away from the TiO_2 anatase (101) surface and $66 \pm 5^{\circ}$ from the TiO_2 rutile (110) surface, suggesting very little difference, within error. The thiol group appears to remain intact and oriented away from the surface, available to interact with other molecules or light-harvesting materials.

Supplementary Materials: The following supporting information can be downloaded at: https://www.mdpi.com/article/10.3390/surfaces5020017/s1: Figure S1: simple two-layer model used in the calculation of surface coverage of MBA on the two titania surfaces. d_A is the thickness of the MBA overlayer. A is MBA and B the titania crystal. References [20,36] are cited in Supplementary Material file.

Author Contributions: Conceptualization, A.G.T.; Formal analysis, C.L.C.-G.; Investigation, C.L.C.-G., A.G.T., K.L.S. and J.C.; Resources, Z.L.; Supervision, A.G.T.; Writing—original draft, C.L.C.-G.; Writing—review & editing, A.G.T., K.L.S., J.C. and Z.L. All authors have read and agreed to the published version of the manuscript.

Funding: The authors acknowledge funding via CALIPSOPlus under the Grant Agreement 730872 from the EU Framework Programme for Research and Innovation HORIZON 2020. C.L.C.-G acknowledges funding of a studentship from Mexican Institutions CONACYT/SENER No 472709. JC acknowledges funding of a studentship from The Jeremiah Horrocks Institute, University of Central Lancashire.

Institutional Review Board Statement: Not applicable for studies not involving humans or animals.

Informed Consent Statement: Not applicable.

Data Availability Statement: Raw data used in this publication is available at https://figshare.manchester.ac.uk/projects/Adsorption_of_mercaptobenzoic_acid_on_the_anatase_101_and_rutile_110_TiO2_surfaces/136301.

Acknowledgments: The authors thank the MATLINE Beamline at ASTRID Synchrotron, Aarhus University, Denmark and the CALIPSO plus project funded under the Grant Agreement 730,872 from the EU Framework Programme for Research and Innovation HORIZON 2020 for the beamtime awarded under project ISA-19-105, Mexican Institutions CONACYT/SENER for the Ph.D. scholarship support for Claudia Lorena Compeán González No 472709, and The Department of Materials, Photon Science Institute and Sir Henry Royce Institute, The University of Manchester, for additional funding.

Conflicts of Interest: The authors declare no conflict of interest.

References

1. Fierro, J.L.G. *Metal Oxides: Chemistry and Applications*; CRC Press: Boca Raton, FL, USA, 2005.
2. Limo, M.J.; Sola-Rabada, A.; Boix, E.; Thota, V.; Westcott, Z.C.; Puddu, V.; Perry, C.C. Interactions between Metal Oxides and Biomolecules: From Fundamental Understanding to Applications. *Chem. Rev.* **2018**, *118*, 11118–11193. [CrossRef] [PubMed]
3. Wright, M.; Uddin, A. Organic—Inorganic hybrid solar cells: A comparative review. *Sol. Energy Mater. Sol. Cells* **2012**, *107*, 87–111. [CrossRef]
4. Parayil, S.K.; Baltrusaitis, J.; Wu, C.-M.; Koodali, R.T. Synthesis and characterization of ligand stabilized CdS-Trititanate composite materials for visible light-induced photocatalytic water splitting. *Int. J. Hydrogen Energy* **2013**, *38*, 2656–2669. [CrossRef]
5. Diebold, U. The surface science of titanium dioxide. *Surf. Sci. Rep.* **2003**, *48*, 53–229. [CrossRef]
6. Park, H.; Park, Y.; Kim, W.; Choi, W. Surface modification of TiO_2 photocatalyst for environmental applications. *J. Photochem. Photobiol. C* **2012**, *15*, 1–20. [CrossRef]

7. Pang, C.L.; Lindsay, R.; Thornton, G. Chemical reactions on rutile TiO_2(110). *Chem. Soc. Rev.* **2008**, *37*, 2328–2353. [CrossRef] [PubMed]
8. Thomas, A.G.; Syres, K.L. Adsorption of organic molecules on rutile TiO_2 and anatase TiO_2 single crystal surfaces. *Chem. Soc. Rev.* **2012**, *41*, 4207–4217. [CrossRef]
9. Moulé, A.J.; Chang, L.; Thambidurai, C.; Vidu, R.; Stroeve, P. Hybrid solar cells: Basic principles and the role of ligands. *J. Mater. Chem.* **2011**, *22*, 2351–2368. [CrossRef]
10. Faure, E.; Falentin-Daudré, C.; Jérôme, C.; Lyskawa, J.; Fournier, D.; Woisel, P.; Detrembleur, C. Catechols as versatile platforms in polymer chemistry. *Prog. Polym. Sci.* **2012**, *38*, 236–270. [CrossRef]
11. Khalid, W.; El Helou, M.; Murböck, T.; Yue, Z.; Montenegro, J.-M.; Schubert, K.; Göbel, G.; Lisdat, F.; Witte, G.; Parak, W.J. Immobilization of Quantum Dots via Conjugated Self-Assembled Monolayers and Their Application as a Light-Controlled Sensor for the Detection of Hydrogen Peroxide. *ACS Nano* **2011**, *5*, 9870–9876. [CrossRef]
12. Becker-Koch, D.; Albaladejo-Siguan, M.; Lami, V.; Paulus, F.; Xiang, H.; Chen, Z.; Vaynzof, Y. Ligand dependent oxidation dictates the performance evolution of high efficiency PbS quantum dot solar cells. *Sustain. Energy Fuels* **2019**, *4*, 108–115. [CrossRef]
13. Beygi, H.; Sajjadi, S.A.; Babakhani, A.; Young, J.F.; van Veggel, F.C. Air exposure oxidation and photooxidation of solution-phase treated PbS quantum dot thin films and solar cells. *Sol. Energy Mater. Sol. Cells* **2019**, *203*, 110163. [CrossRef]
14. Sánchez-Sánchez, C.; Martín-Gago, J. *Adsorption and Self-Assembly of Organic Molecules on TiO_2 Substrates*; Elsevier: Amsterdam, The Netherlands, 2018; pp. 1–12. [CrossRef]
15. Inerbaev, T.M.; Masunov, A.E.; Khondaker, S.I.; Dobrinescu, A.; Plamadă, A.-V.; Kawazoe, Y. Quantum chemistry of quantum dots: Effects of ligands and oxidation. *J. Chem. Phys.* **2009**, *131*, 044106. [CrossRef]
16. Lee, J.R.I.; Willey, T.M.; Nilsson, J.; Terminello, L.J.; De Yoreo, J.J.; van Buuren, T. Effect of Ring Substitution Position on the Structural Conformation of Mercaptobenzoic Acid Self-Assembled Monolayers on Au(111). *Langmuir* **2006**, *22*, 11134–11141. [CrossRef]
17. Hou, W.; Setvin, M.; Schmid, M.; Aschauer, U.J.; Diebold, U.; Selloni, A.; Li, Y.-F.; Scheiber, P. Reaction of O_2 with Subsurface Oxygen Vacancies on TiO_2 Anatase (101). *Science* **2013**, *341*, 988–991. [CrossRef]
18. Quah, E.L.; Wilson, J.N.; Idriss, H. Photoreaction of the Rutile TiO_2(011) Single-Crystal Surface: Reaction with Acetic Acid. *Langmuir* **2010**, *26*, 6411–6417. [CrossRef]
19. Syres, K.L.; Thomas, A.G.; Graham, D.M.; Spencer, B.F.; Flavell, W.R.; Jackman, M.J.; Dhanak, V.R. Adsorption and stability of malonic acid on rutile TiO_2 (110), studied by near edge X-ray absorption fine structure and photoelectron spectroscopy. *Surf. Sci.* **2014**, *626*, 14–20. [CrossRef]
20. Powell, C.; Jablonski, A. *NIST Electron Effective-Attenuation-Lenght Database, SRD82*; U.S. Department of Commerce: Gaithersburg, MD, USA, 2011.
21. Syres, K.; Thomas, A.; Bondino, F.; Malvestuto, M.; Grätzel, M. Dopamine Adsorption on Anatase TiO_2(101): A Photoemission and NEXAFS Spectroscopy Study. *Langmuir* **2010**, *26*, 14548–14555. [CrossRef]
22. Hermann, K.; Pettersson, L. *StoBe-deMon Software*, Version 2.2 of deMon. 2006.
23. Jackman, M.J.; Thomas, A.G.; Muryn, C. Photoelectron Spectroscopy Study of Stoichiometric and Reduced Anatase TiO_2(101) Surfaces: The Effect of Subsurface Defects on Water Adsorption at Near-Ambient Pressures. *J. Phys. Chem. C* **2015**, *119*, 13682–13690. [CrossRef]
24. Thomas, A.G.; Jackman, M.J.; Wagstaffe, M.; Radtke, H.; Syres, K.; Adell, J.; Lévy, A.; Martsinovich, N. Adsorption Studies of p-Aminobenzoic Acid on the Anatase TiO_2(101) Surface. *Langmuir* **2014**, *30*, 12306–12314. [CrossRef]
25. Schnadt, J.; O'Shea, J.; Patthey, L.; Schiessling, J.; Krempaský, J.; Shi, M.; Mårtensson, N.; Brühwiler, P. Structural study of adsorption of isonicotinic acid and related molecules on rutile TiO_2(110) II: XPS. *Surf. Sci.* **2003**, *544*, 74–86. [CrossRef]
26. Hashimoto, S.; Tanaka, A. Alteration of Ti 2p XPS spectrum for titanium oxide by low-energy Ar ion bombardment. *Surf. Interface Anal.* **2002**, *34*, 262–265. [CrossRef]
27. Pang, C.L.; Lindsay, R.; Thornton, G. Structure of Clean and Adsorbate-Covered Single-Crystal Rutile TiO_2 Surfaces. *Chem. Rev.* **2013**, *113*, 3887–3948. [CrossRef] [PubMed]
28. Hermann, K.; Pettersson, L.G.M.; Casida, M.E.; Daul, C.; Goursot, A.; Koester, A.; Proynov, E.; St-Amant, A.; Salahub, D.R.; Carravetta, V.; et al. *StoBe-deMon*, Version 3.3. 2014.
29. Neese, F. The ORCA program system. *Wiley Interdiscip. Rev. Comput. Mol. Sci.* **2012**, *2*, 73–78. [CrossRef]
30. Neese, F. Software update: The ORCA program system, version 4.0. *Wiley Interdiscip. Rev. Comput. Mol. Sci.* **2018**, *8*, e1327. [CrossRef]
31. Hanwell, M.D.; Curtis, D.E.; Lonie, D.C.; Vandermeersch, T.; Zurek, E.; Hutchison, G.R. Avogadro: An advanced semantic che-mical editor, visualization, and analysis platform. *J. Cheminform.* **2012**, *4*, 17.
32. Thomas, A.G.; Flavell, W.R.; Kumarasinghe, A.R.; Mallick, A.K.; Tsoutsou, D.; Smith, G.C.; Stockbauer, R.; Patel, S.; Grätzel, M.; Hengerer, R. Resonant photoemission of anatase (formula presented) (101) and (001) single crystals. *Phys. Rev.-Condens. Matter Mater. Phys.* **2003**, *67*, 035110. [CrossRef]
33. Thomas, A.G.; Flavell, W.R.; Mallick, A.K.; Kumarasinghe, A.R.; Tsoutsou, D.; Khan, N.; Chatwin, C.; Rayner, S.; Smith, G.C.; Stockbauer, R.L.; et al. Comparison of the electronic structure of anatase and rutile TiO_2 single-crystal surfaces using resonant photoemission and x-ray absorption spectroscopy. *Phys. Rev. B.* **2007**, *75*, 035105. [CrossRef]

34. Jackman, M.J.; Syres, K.L.; Cant, D.J.H.; Hardman, S.J.O.; Thomas, A.G. Adsorption of Dopamine on Rutile TiO_2 (110): A Photoemission and Near-Edge X-ray Absorption Fine Structure Study. *Langmuir* **2014**, *30*, 8761–8769. [CrossRef]
35. Stöhr, J. *NEXAFS Spectroscopy*; Gomer, R.L., Mills, D., Eds.; Springer Science & Business Media: Berlin/Heidelberg, Germany, 1992; Volume 25.
36. Briggs, D.; Seah, M.P. *Practical Surface Analysis (Second Edition), Volume 1—Auger and X-ray Photoelectron Spectroscopy*, 2nd ed.; John Wiley and Sons Ltd.: Chichester, UK, 1990.